Available online at www.sciencedirect.com
ScienceDirect
Trans. Nonferrous Met. Soc. China 34(2024) 2245−2259
Transactions of Nonferrous Metals Society of China
www.tnmsc.cn

A unified constitutive model of FCC metal in ultrasonic vibration with application to oxygen-free high-thermal conductivity copper

Peng-fei SONG[1,2], Miao-yan CAO[1,2], Han HU[1,2], Ji-ye CHEN[3], Min FU[1,2]

1. School of Mechanical Engineering, Yanshan University, Qinhuangdao 066004, China;
2. Hebei Light Structural Equipment Design and Manufacturing Technology Innovation Center, Yanshan University, Qinhuangdao 066004, China;
3. School of Civil Engineering and Surveying, University of Portsmouth, Portsmouth PO1 3AH, UK

Received 6 January 2023; accepted 26 July 2023

Abstract: A unified constitutive model is established to predict the plastic flow behavior of face-centered cubic (FCC) metal in the ultrasonic vibration (UV) assisted forming. The model describes UV softening behavior based on the dislocation dynamics in the UV combined with the stress superposition mechanism. The interaction among dislocation density, grain size and UV is considered, and the residual behavior of UV-assisted forming can be predicted by modelling with dislocation density and grain size as internal state variables. UV-assisted compression tests were performed on oxygen-free high-thermal conductivity (OFHC) copper to verify the predictive ability of the model. The results show that OFHC copper exhibits obvious softening behavior and residual softening behavior in the UV. The model prediction is in good agreement with the experimental result, which effectively captures the softening effect and residual effect of copper.

Key words: constitutive modelling; ultrasonic vibration; acoustic softening behavior; compression; copper

1 Introduction

Ultrasonic vibration (UV) assisted forming is an advanced high-energy rate-forming technology that can enhance the surface quality of a workpiece and improve the forming properties and precision of a material [1]. However, the wide application of the UV in various manufacturing processes poses a serious challenge to the design guidance of ultrasonic instruments and process optimization. Numerical simulation is a more efficient and economical approach to this problem than costly experimental trial-and-error methods. Therefore, there has been a growing interest in the definition of a reliable UV constitutive models for numerical analysis.

The influence of UV on the structure and performance of the workpieces depends on the surface and volume effects. The former refers to the friction between the mold and blank, which must be considered to design ultrasonic instruments in various forming processes, and the latter refers to the softening and residual phenomena due to UV-induced stress and strain, which is closely related to the dynamic behavior of a metal in the UV [1]. In response to the description of vibration-induced material mechanical behavior, YAO et al [2] proposed a unified acoustic plasticity model (Yao model) by attributing acoustic softening to changes in frequency factor and activation energy using the thermally activated Arrhenius equation and acoustic residual effects on dislocation evolution. However, the potential barriers that prevent dislocation motion

Corresponding author: Miao-yan CAO, Tel: +86-335-8061730, E-mail: jacmy@ysu.edu.cn
DOI: 10.1016/S1003-6326(24)66538-6

can be divided into long-range and short-range potential barriers according to the dislocation dynamics theory [3]. Unfortunately, the Yao model does not take into account the nonthermal activated motion of the dislocations. SEDAGHAT et al [4] presented an acoustic plasticity constitutive model (Sedaghat model) by considering dislocation dynamics and acoustic energy transformation mechanisms, which successfully simulated the compression forming, press forming, and incremental forming under UV. ZHAO and WU [5] developed a new model (Zhao model) by considering acoustic stress work and combining the Sellars Tegart and Gao−Zhang models, which effectively predicted the flow stresses of the aluminum alloy in the UV (20 kHz) friction stir welding process. Although the Sedaghat and Zhao models complemented the non-thermally activated components, the dynamic behavior in the UV is closely related to its microstructural evolution, while the effect of the UV on microstructure evolution was neglected in the models. In addition, MENG et al [6] developed a hybrid constitutive model (Meng model) by considering the influence of the UV on the non-thermally dislocations motion based on the dislocation evolution theory, which distinguishes between stress superposition and the acoustic softening effect. WANG et al [7] developed an energy-based model (Wang model) by considering that the non-thermally dislocation dynamics heterogeneously change at the micro-structure level in the UV. The research results of MENG et al [6] and WANG et al [7] indicated that UV can assist the non-thermally activated dislocations motion, which were not considered in the Yao, Sedaghat, and Zhao models. However, the Meng and Wang models ignored dislocation motion across the short-range barriers in the UV assisted forming. The interpretation of acoustic softening phenomenon requires a comprehensive consideration of the effect of ultrasonic energy on thermally and non-thermally activated dislocation motions based on the above literature survey, which has so far been barely considered in existing models.

Notably, several observations have shown that UV has a remarkable effect on the microstructure evolution. The UV can enhance recrystallization in the middle of the horizontal molten core region of the AA6061-T6 alloy, induce grain refinement in aluminum (AA5754 alloy), and increase the dislocation multiplication speed of pure aluminum (Al1100) [2,8,9]. On the contrary, UV can also enhance the migration and disappearance of twin boundaries and reduce the geometrically necessary dislocation density of copper [10]. The above is also one of the reasons for the residual effects following the discontinuity in the UV. However, the acoustic plastic behavior was captured in most models through a single structural parameter (dislocation density) evolution, whereas the recrystallization or grain growth behavior induced by the UV is barely considered. In particular, the modelling mechanisms of interaction among the ultrasound energy field, the dislocation density evolution and the grain evolution are still lacking.

Therefore, in this study, a new dislocation dynamics-based acoustic plasticity framework is developed to describe the dynamical behavior of FCC metals in the UV. The framework considers thermally and non-thermally activated dislocation motions, stress superposition mechanisms, and the evolution of dislocation density and grain size in UV assisted forming. An UV assisted compression experiment using OFHC copper is conducted, and the microstructure of the samples in the UV assisted forming is analyzed by X-ray diffraction (XRD) and metallographic microscopy to validate the reliability of the model.

2 Model framework

2.1 Kinematics under ultrasonic energy field

The macroscopic plastic response of metals is determined by the mechanisms related to the dislocation motion, the substructure evolution, the distribution of barriers preventing dislocation movement, and the relationship between externally imposed plastic strain rate and dislocation kinetics [11]. According to the kinetics theory, the strain rate ($\dot{\varepsilon}$) can be expressed as [4]

$$\dot{\varepsilon}=\dot{\gamma}/M=\rho_{\mathrm{m}}b\overline{v}/M \tag{1}$$

where $\dot{\gamma}$ is the shear plastic strain rate, $M(=\sigma/\tau=\gamma/\varepsilon$, σ and ε are the flow stress and plastic strain, and τ and γ are the critical resolved shear stress and shear strain in the active slip system, respectively) is the Taylor factor, which is always taken as an empirical value of 3.06 for FCC metals [12], ρ_{m} is the mobile

dislocation density, b is the magnitude of Burgers vector, and $\overline{v}$ is the average speed of dislocation. Notably, three different mechanisms (i.e., thermally activated dislocation movement, dislocation drag mechanisms, relativistic effects) for controlling metal plastic deformation have been consistently acknowledged. Therefore, it is necessary to identify rate-controlled deformation mechanisms in the UV.

The vibrational shape is assumed to conform to a sinusoidal function. When the specimen is only exposed to force in the direction of tension/compression and the longitudinal UV excitation is employed (i.e., the direction of vibration excitation is parallel to the force applied to the specimen), the strain history can be assessed by the superposition method. Hence, the strain rate under the UV ($\dot{\varepsilon}$) can be roughly expressed as [13]

$$\dot{\varepsilon}=\dot{\varepsilon}_0+2\pi Af\left|\cos(2\pi ft)\right|/l_{\mathrm{d}} \tag{2}$$

where $\dot{\varepsilon}_0$ is the strain rate without the UV, A and f represent the amplitude and the frequency, respectively, t is the time, and l_{d} is the length of the specimen involving the deformation. The frequency and amplitude used in conventional machining are 20−40 kHz, and within 20 μm, respectively [14]. Some studies have shown that plastic deformation is still controlled by the thermally activated dislocation mechanisms when the strain rate approaches $10^4\ \mathrm{s}^{-1}$ [15]. A rough estimate by Eq. (2) showed that the strain rate in the UV can reach $10^4\ \mathrm{s}^{-1}$ if $l_{\mathrm{d}}<0.05$ mm. However, $l_{\mathrm{d}}\gg 0.05$ mm in conventional deformation. Therefore, this study considers that the rate control mechanism in conventional UV is only thermally activated dislocation movement.

It will encounter periodic potential barriers with different intervals and lengths when dislocation moves in the lattice, which can be divided into two types: short-range and long-range barriers. The former can be overcome by thermal energy and belongs to the thermal activation type, whereas the latter cannot [16]. The flow stress (τ) can be expressed accordingly as

$$\tau=\tau_{\mathrm{th}}+\tau_{\mathrm{ath}} \tag{3}$$

where τ_{th} and τ_{ath} represent the thermally activated component and the non-thermally activated component of the flow stress, respectively. The role of the UV is to impose mechanical vibration on the sample, resulting in an elastic deformation at ultrasonic frequency. It is well known that elastic deformation is determined by interatomic binding forces. The superposition of the UV alters the interatomic interaction forces, leading to a reduction of the binding energy, which affects the energy barriers that prevent dislocation movement. For FCC metals, the barriers are mainly provided by forest dislocations (short-range barriers) and grain boundaries (long-range barriers). Therefore, the effect of UV on the interaction processes of dislocations with forest dislocations and grain boundaries should be considered simultaneously in order to clearly describe the plastic response behavior in the UV.

2.2 Thermally activated dislocation movement under ultrasonic energy field

Based on the thermally activated theory, the shear plastic strain rate ($\dot{\gamma}$) can also be expressed as [4]

$$\dot{\gamma}=\dot{\gamma}_{\mathrm{p}}\exp[-\Delta G/(kT)] \tag{4}$$

where $\dot{\gamma}_{\mathrm{p}}$ is the pre-exponential factor, ΔG is the activation energy, k is the Boltzmann constant, and T represents thermodynamic temperature. KLEPACZKO [17] pointed out that the required energy ΔW_{t} of dislocation motion across the short-range barriers is a combination of external work ΔW and activation energy ΔG, that is, $\Delta W_{\mathrm{t}}=\Delta G+\Delta W$. The superposition of UV can provide additional energy, resulting in the effective height of the short-range barriers being further reduced. Therefore, according to the nonlinear stress-dependent activation energy model proposed by KOCKS [18], the activation energy under the UV can be expressed as

$$\Delta G=\Delta G_0\left[1-\left(\tau_{\mathrm{th}}/\hat{\tau}_{\mathrm{th}}\right)^p\right]^q-\Delta W_{\mathrm{uth}} \tag{5}$$

where $\Delta G_0(=g_0\mu b$, g_0 is nominal activation energy) is the reference activation energy, μ is the shear modulus, p and q are the parameters characterizing the shape of the activation energy barrier ($0<p\leq 1$, $1\leq q\leq 2$), $\hat{\tau}_{\mathrm{th}}(=\Delta G_0\sqrt{\rho_{\mathrm{m}}}/b^2)$ is the thermally activated stress at 0 K (i.e., mechanical threshold stress), and ΔW_{uth} represents the activation energy net-change caused by the UV. By making the proper substitutions in Eq. (4), the thermally activated stress under UV (τ_{th}) can be written as

$$\tau_{\mathrm{th}}=\hat{\tau}_{\mathrm{th}}\left\{1-\left[\left(\Delta W_{\mathrm{uth}}-(kT\ln(\dot{\gamma}/\dot{\gamma}_{\mathrm{p}}))/\Delta G_0\right]^{1/q}\right\}^{1/p} \tag{6}$$

2.3 Non-thermally activated dislocation movement under ultrasonic energy field

The non-thermally activated component of the flow stress assists the dislocation movement to cross the long-range barriers, which can be expressed as [15]

$$\tau_{ath}=\tau_0+\tau_{sd}=\tau_0+k_s d^{-1/2} \tag{7}$$

where τ_0 is the stress due to initial defects, τ_{sd} is the stress induced by the size effect, k_s represents the Hall–Petch slope, and d is the mean grain diameter. The grain size stress τ_{sd} can be taken as a constant for a given material if no physical changes occur during plastic deformation. As described in the introduction, τ_{sd} in the UV cannot be taken as a constant. Unfortunately, the physical meaning of k_s has not been clearly defined so far. However, research [7] showed that the physical meaning explained by the use of energy-based models is more applicable to the study of the mechanical response mechanisms in the UV. Therefore, k_s is used to measure the energy required to eject dislocations from a grain boundary, and τ_{sd} can be expressed as

$$\tau_{sd}=2\Delta W_e\sqrt[4]{\rho_{gb}}/(b\sqrt{d}) \tag{8}$$

where ΔW_e represents the energy that ejects the dislocations from the grain boundary, and ρ_{gb} is the dislocation density in the grain boundary. Based on the linear elastic dislocation theory [19] and considering that UV can improve the probability of the dislocation crossing the long-range barrier, the dislocation-ejecting energy under the UV can be expressed as

$$\Delta W_e=-\Delta W_{uath}+\left[0.25\xi_1\mu b^2\ln\left(b^{\xi_2-1}\rho_{gb}^{\xi_2/2}/\sqrt{\rho_{gi}}\right)/\pi\right] \tag{9}$$

where ΔW_{uath} represents the ejecting energy net-change caused by the UV in the driving dislocation motion crossing long-range barrier, ξ_1 is material constant, ξ_2 is a modified factor, which is introduced to neglect the effect of dislocation orientation and overall dislocation configuration in the grain boundary (ξ_2=0.45 for grains over 5 μm [20]), and ρ_{gi} is the dislocation density in grain interior. By making the proper substitutions in Eq. (7), the non-thermally activated stress under UV can be expressed as

$$\tau_{ath}=\tau_0+\xi_1\mu b\sqrt[4]{\rho_{gb}}\ln\left(b^{\xi_2-1}\rho_{gb}^{\xi_2/2}/\sqrt{\rho_{gi}}\right)/(2\pi\sqrt{d})-2\Delta W_{uath}\sqrt[4]{\rho_{gb}}/(b\sqrt{d}) \tag{10}$$

The reduction of flow stress in the UV is proportional to the ultrasonic energy density or intensity (or the square of the acoustic energy density) [15]. It is considered that different types of obstacles have different responses to the ultrasonic energy field, so the energy net-change can be expressed as

$$\Delta W_{uth}=\beta_{uth}\left(S_a I_{uv}\right)^{n_{uth}} \tag{11}$$

$$\Delta W_{uath}=\beta_{uath}\left(S_a I_{uv}\right)^{n_{uath}} \tag{12}$$

where β_{uth}, β_{uath}, n_{uth}, n_{uath} are the constants associated with the barriers that impede dislocation movement, S_a is the sample cross-sectional area, and I_{uv} is the ultrasound energy intensity, which can be expressed as

$$I_{uv}=0.5\alpha_{uv}A_h^2\omega^2\rho_{mc1}c_{uv1} \tag{13}$$

where $\alpha_{uv}(=4\rho_{mc1}c_{uv1}\rho_{mc2}c_{uv2}(\rho_{mc1}c_{uv1}+\rho_{mc2}c_{uv2})^{-2})$ is the ultrasound intensity transmissivity at different interfaces, A_h is the vibrating tool head amplitude, $\omega(=2\pi f)$ is the ultrasound angular frequency, ρ_{mci} (i=1, 2) is the medium density, $c_{uvi}(=\sqrt{E/\rho_{mci}})$ (i= 1, 2) represents the acoustic velocity, and E is the elasticity modulus [21].

In addition, the softening effect is also associated with the ultrasonic frequency loading/unloading circulations (i.e., stress superposition mechanism). As the UV is applied to the material, a periodic loading/unloading of the material is performed tens of thousands of times per second, generating strain fluctuations that lead to a reduction in the average stress. The stress reduction generated by the stress superimposition can be expressed as [22]

$$\Delta\tau_{su}=\xi_{su}\left(S_a I_{uv}\right)^{n_{su}} \tag{14}$$

where ξ_{su} and n_{su} are parameters related to the ultrasound energy field. Equations (3), (6), (10) and (14) describe the softening effect of the UV using dislocation kinematics and stress superposition mechanisms.

2.4 Substructure evolution under ultrasonic energy field

The dynamical behavior of metals in the UV is closely related to the dislocation evolution during deformation. However, as described in the

introduction, the UV also has a significant effect on grain boundary migration and grain size, and similar phenomena were also found in the microscopic characterization experiments in this study. It has been shown that grain size and shape have a significant effect on the properties of a material [23]. Therefore, it is necessary to consider the grain evolution behavior, which has been neglected in most of the ultrasonic energy field modelling in order to accurately and unambiguously describe the microstructural evolution behavior in the UV.

2.4.1 Dislocation density

The normalized dislocation density law (NDD) [24] in the cold forming formation can be expressed as

$$\dot{\bar{\rho}} = \alpha_0 \left| \dot{\gamma}^p \right| - \alpha_0 \bar{\rho}^{\varsigma_{\bar{\rho}0}} \left| \dot{\gamma}^p \right| \tag{15}$$

where $\bar{\rho} = (\rho_{\text{tot}} - \rho_{\text{i}})/\rho_{\text{s}}$, ρ_{tot} is the mean dislocation density, ρ_{i} is the initial dislocation density (annealed state), and ρ_{s} is the saturated dislocation density. It should be noted that the assumption that the total dislocation density and mobile dislocation density are approximately equal is adopted (i.e., $\rho_{\text{tot}} \approx \rho_{\text{m}}$) in this study due to the fact that the mobile dislocation density is not easily identified directly. Actually, the assumption has been used in the models of Haasen and Gao, respectively [15,25]. The term on the right-hand side of Eq. (15) represents dislocation storage and dynamic recovery, respectively, $\alpha_0 (\propto (M/bL))$ is regarded as a constant, and L is the average glide distance between successive obstacles on the slip planes. $\varsigma_{\bar{\rho}0}$ is material constant. The influence of the UV on dislocation density is normalized by introducing a new term, $f(\bar{\rho})$, to circumvent the difficulty of determining the exact effect of the UV independently, that is

$$\dot{\bar{\rho}} = \alpha_0 \left(1 - \bar{\rho}^{\varsigma_{\bar{\rho}0}}\right) \left| \dot{\gamma}^p \right| + f(\bar{\rho}) \tag{16}$$

The last term on the right-hand side of Eq. (16) represents the effect of UV. Metals with the same FCC crystal structure exhibit different mechanical phenomena in the UV. For example, aluminum alloys (high stacking fault energy) and copper (medium stacking fault energy) exhibit residual hardening and softening, respectively [10,15]. It is well known that the stacking fault energy is the primary factor affecting the dislocation slip pattern. Therefore, different residual phenomena described above can be attributed to the different effects of the UV on the dislocation slip modes in materials with different stacking fault energies. Then, the UV effect can be expressed as

$$f(\bar{\rho}) = \pm \alpha_1 \eta_\rho \bar{\rho}^{\varsigma_{\bar{\rho}1}} \left| \dot{\gamma}^p \right| \tag{17}$$

where sign "+" ("−") represents the additional multiplication (annihilation) induced by the UV, α_1 and $\varsigma_{\bar{\rho}_1}$ are the material constants, and η_ρ reflects the UV dependence of the dislocation evolution at a given plastic strain. A typical logistic function is appropriate to describe the UV induced dislocation evolution behavior considering the saturation behavior of the residual effect [2]. Hence, η_ρ can be expressed as

$$\eta_\rho = \eta_\rho^0 \eta_\rho^{\text{S}} / [\eta_\rho^0 + (\eta_\rho^{\text{S}} - \eta_\rho^0) \exp(-\Theta_\rho t_{\text{uv}})] \tag{18}$$

where η_ρ^0 and η_ρ^{S} are the initial and the saturation value of η_ρ, respectively, the parameter $\Theta_\rho (= \gamma_\rho I_{\text{uv}})$ represents the growth rate, which is related to ultrasound energy intensity, and t_{uv} is the UV duration.

2.4.2 Grain size

There are similarities between thermal deformation and UV assisted deformation on the microstructure evolution [26]. The evolutionary law of the average grain size in thermal deformation can generally be expressed as [27]

$$\dot{d} = \beta_1 d^{-\varsigma_{\text{d1}}} + \beta_2 \left| \dot{\gamma} \right| d^{-\varsigma_{\text{d2}}} - \beta_3 \dot{S}^{\varsigma_{\text{d3}}} d^{\varsigma_{\text{d4}}} \tag{19}$$

where β_1, ς_{d1}, β_2, ς_{d2}, β_3, ς_{d3}, ς_{d4} are material constants, $\dot{S}$ is the evolution of recrystallized volume fraction. The first two terms represent static and dynamic grain growth, respectively, and the last term describes the grain refinement caused by the recrystallization. The evolution of recrystallized volume fraction can be expressed as

$$\dot{S} = \xi_{\dot{\text{S}}} \left[x\bar{\rho} - \bar{\rho}_{\text{c}} (1 - S) \right] (1 - S)^{n_{\dot{\text{S}}}} \tag{20}$$

where $\xi_{\dot{\text{S}}}$ and $n_{\dot{\text{S}}}$ are material constants, x is the incubation factor for the start of recrystallization, which can be expressed as

$$\dot{x} = \beta_x (1 - x) \bar{\rho} \tag{21}$$

where β_x is a materiel constant, and $\bar{\rho}_{\text{c}}$ is the critical value of the normalized dislocation density. Recrystallization is closely related to the dislocation density, and the deformed material may begin to crystallize under the excitation of UV when the dislocation density increases to a fairly high level. The UV effect on the recrystallization can then be introduced by changing the dislocation density.

Therefore, the behavior of grain evolution in the UV consists of dynamic grain growth, grain refinement due to recrystallization, and dynamic grain growth induced by the ultrasonic energy field, which can be expressed as

$$\dot{d}=\beta_2|\dot{\gamma}|d^{-\varsigma_{d2}}-\beta_3\dot{S}^{\varsigma_{d3}}d^{\varsigma_{d4}}+\beta_4\eta_d|\dot{\gamma}|d^{\varsigma_{d5}} \tag{22}$$

where the last term of Eq. (22) represents the dynamic grain growth induced by the UV, β_4 and ς_{d5} are material constants, and η_d represents the dependence of grain growth on ultrasonic energy field, which can also be expressed as

$$\eta_d=\eta_d^0\eta_d^S/\left(\eta_d^0+(\eta_d^S-\eta_d^0)\exp(-\Theta_d t_{uv})\right) \tag{23}$$

where $\Theta_d=\gamma_d I_{uv}$. Recrystallization, in turn, can affect dislocation segments. It is generally considered that there are no dislocations when a new grain is nucleated, that is, recrystallization reduces the dislocation density [27]. Then, the dislocation density evolution in the UV needs to be modified as follows:

$$\dot{\overline{\rho}}=\alpha_0\left(1-\overline{\rho}^{\varsigma_{\overline{\rho}0}}\right)|\dot{\gamma}^p|\pm\alpha_1\eta_\rho\overline{\rho}^{\varsigma_{\overline{\rho}1}}|\dot{\gamma}^p|-\alpha_2\overline{\rho}\dot{S}/(1-S) \tag{24}$$

where α_2 is material constant. The above equations provide a theoretical framework for residual effects in the UV based on the evolution theory of dislocation density and grain size.

2.5 Formulation of unified acoustic plastic constitutive model

The unified acoustic plastic constitutive model is developed to model the motion of dislocations across short- and long-range barriers, the evolution of dislocation density and grain size in the UV of FCC metals, and to reasonably account for the effects of these evolutions on the plastic flow behavior and its internal relations. The unified acoustic plastic constitutive equations are listed in Eq. (25):

$$\begin{cases}\tau=\tau_{ath}+\tau_{th}-\Delta\tau_{su}\\ \tau_{ath}=\tau_0-2\Delta W_{uath}\sqrt[4]{\rho_{gb}}/(b\sqrt{d})+\\ \qquad\xi_1\mu b\sqrt[4]{\rho_{gb}}\ln(b^{\xi_2-1}\rho_{gb}^{\xi_2/2}\rho_{gi}^{-0.5})/(2\pi\sqrt{d})\\ \tau_{th}=\hat{\tau}_{th}\left\{1-\left[(\Delta W_{uth}-kT\ln(\dot{\gamma}/\dot{\gamma}_p))/\Delta G_0\right]^{1/q}\right\}^{1/p}\\ \Delta\tau_{su}=\xi_{su}(S_aI_{uv})^{n_{su}}\\ \dot{\overline{\rho}}=\alpha_0(1-\overline{\rho}^{\varsigma_{\overline{\rho}0}})|\dot{\gamma}^p|\pm\alpha_1\eta_\rho\overline{\rho}^{\varsigma_{\overline{\rho}1}}|\dot{\gamma}^p|-\alpha_2\overline{\rho}\dot{S}/(1-S)\\ \dot{d}=\beta_2|\dot{\gamma}|d^{-\varsigma_{d2}}-\beta_3\dot{S}^{\varsigma_{d3}}d^{\varsigma_{d4}}+\beta_4\eta_d|\dot{\gamma}|d^{\varsigma_{d5}}\end{cases} \tag{25}$$

3 Experimental

3.1 UV assisted compression experiment

The experimental setup for the UV compression is demonstrated in Fig. 1. The UV assisted compression testing system was designed based on a WDW 100 kN universal testing machine (UTM). The UTM controls the compression motion, and an ultrasonic vibrator generates the ultrasonic frequency oscillation applied to the specimen. The ultrasonic vibrator includes a CS−2000E−QC series ultrasonic generator with a maximum power of 3000 W, a piezoceramic transducer with a frequency of 20 kHz, and a horn and a tool head, which are

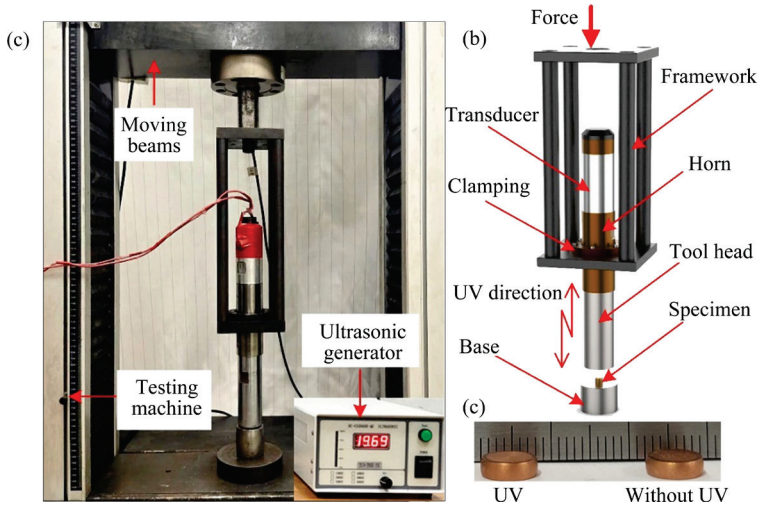

Fig. 1 Equipment of UV assisted compression experimental: (a) WDW 100 kN universal testing; (b) Experimental principle schematic diagram; (c) Compression specimen

fixed by the framework. Ultrasonic oscillation is generated by the ultrasonic generator through the transducer and then the horn, and finally transmitted to the sample by the tool head. The output power of the ultrasonic generator can be changed using the knob in the control panel to apply ultrasonic pulses with different intensities and time to the compression specimens. The amplitudes of the ultrasonic vibrator under different output powers were measured by a digital laser vibrometer. The internal acoustic intensity of the specimen in the UV is difficult to directly measure. Therefore, the internal acoustic intensity is evaluated based on Eq. (13) by measuring the amplitude at the tool head end (where α_{uv} was calculated as 0.9872 based on material properties). The calculation results are given in Table 1.

The compression test was carried out with OFHC copper. The sample size is 5 mm in diameter and 4 mm in length. The compression speed was set to be 1 mm/min in all tests. All the specimens were preloaded to 10 N before the start of the compression test, and each experiment protocol was repeated at least three times to ensure the reliability of the experimental results. Compressed specimens with and without UV are shown in Fig. 1(c).

Table 1 Acoustic intensity under different output powers

Output power/W	Frequency/ kHz	Amplitude/ μm	Acoustic intensity/ (W·mm^{-2})
0	0	0	0
600	19.69	2.93	2.22
1200	19.69	3.6	3.36
1800	19.69	4.29	4.77
2400	19.69	4.95	6.35
3000	19.69	5.65	8.27

3.2 Microstructure observation

Microstructure examination of the specimens undergoing the UV compression are conducted using metallographic microscopy and XRD to investigate the intrinsic mechanism of the softening effect. Optical images were taken with an Axio Scope A1. A standard polishing procedure was followed to prepare the sample for microstructural analysis. Each sample was ground to 2000 grid with SiC paper, then mechanically polished with 1 and 0.5 μm diamond pastes, and finally chemically etched with a solution of 5 g $FeCl_3$, 15 mL HCl, and 85 mL of distilled water.

XRD measurements were conducted with a D/MAX 2500 HB+/PC diffractometer using a Cu target operating voltage of 40 kV with a wavelength λ of 0.15406 Å. The scanning range 2θ was set from 40° to 100° in steps of 0.02° using a stepped scanning mode. Si powder was used as the standard to obtain the instrumental profile function. XRD was used to characterize the average dislocation density within the specimen, which requires a higher surface quality of the sample. Therefore, the standard polishing procedure was also used for XRD sample preparation.

3.3 Results

The several typical true stress−strain curves of OFHC copper in UV assisted compression tests are shown in Fig. 2. Following the application of the UV, the stress−strain curves in the elastic stage

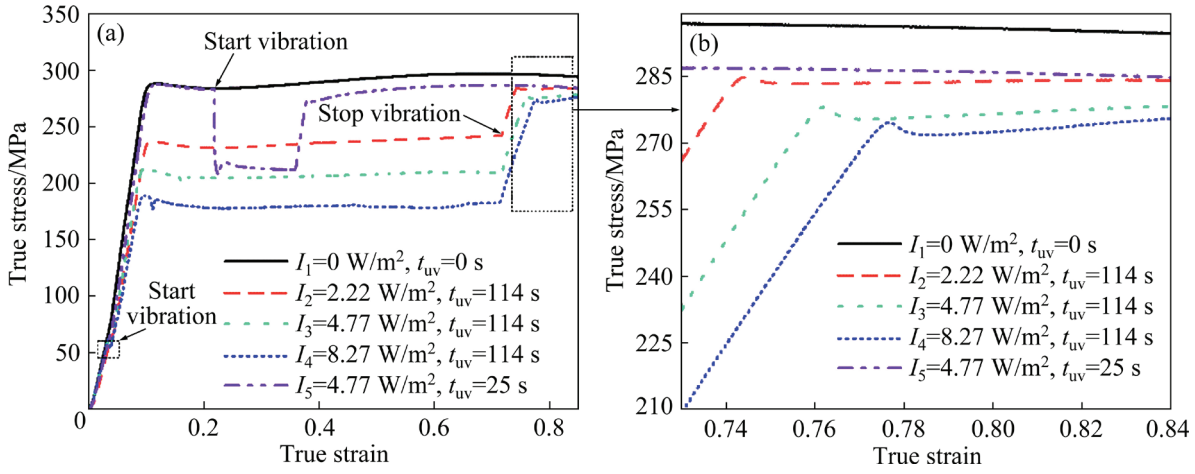

Fig. 2 True stress–strain curves of OFHC copper in UV-assisted compression tests

approximately coincide, while a significant softening phenomenon (i.e., softening effect) can be observed in the plastic stage, and with the increase of acoustic intensity, the degree of softening increases significantly. The softening phenomenon occurs instantly when UV (I_5=4.77 W/mm^2, and t_{uv}=25 s) is applied during the stable plastic deformation. The instant softening phenomenon disappears following the cessation of UV application, and a remarkable residual softening (i.e., acoustic residual effect) is observed. The degree of residual softening increases with increasing acoustic intensity and duration. It is shown that the softening effect is a temporary behavior caused by the UV, whereas the residual effect is a permanent behavior caused by the additional evolution of the UV-induced microstructure.

The mean dislocation density can be evaluated by the modified Williamson−Hall plot [28,29] based on full width at half maximum (FWHM) or integral breadth. Within the kinematical theory of XRD, if the diffraction profile does not undergo the Fourier transform, then the integral width can be expressed as

$$\Delta K = \alpha_k / d + Kb\sqrt{0.5\pi \overline{C} M_d \rho_{tot}} + O(K^2 \overline{C}) \quad (26)$$

where ΔK=2cos $\theta\Delta\theta/\lambda$, α_k=1 for integral width (α_k=0.9 for FWHM), K=2sin θ/λ, $\Delta 2\theta$ is the integral width, M_d(=2.8) is the dislocation arrangement parameter [29], and O stands for higher-order term in $K\overline{C}^{1/2}$, which is considered to be negligible. The Fourier analysis method [30] is used to subtract the effect of instrumentation on the peak breadth of the spectral lines. The FWHMs of the {111}, {200}, {220}, and {311} peaks of the OFHC copper samples under different UV conditions are plotted in Fig. 3(a). The evaluated results are shown in Fig. 3(b). The mean dislocation density decreases from 2.72×10^{14} m^{-2} under conventional deformation to 1.67×10^{14} m^{-2} after the superimposition of UV (I_4=8.27 W/mm^2, and t_{uv}=114 s). It is indicated that the residual softening behavior of OFHC copper is related to the decrease of dislocation density. In addition, the amplitude of the decrease of the mean dislocation density with increasing ultrasound energy decreases from 0.46 for I_3 to 0.27 for I_4, indicating to some extent a saturation effect of the UV effect on the microstructure.

The optical images of the OFHC copper without UV and with UV are shown in Fig. 4. Distinguishing differences in the mean grain diameter can be clearly identified between the images. The mean grain size was estimated using the orthogonal intercept method according to ASTM E112. Results show that the mean grain sizes of OFHC copper are 10.1 μm after the deformation with UV and 7.8 μm without UV. In comparison, the mean grain size increases in UV, although the samples undergo the same deformation. ZHANG et al [31] found that the grain structure of copper was significantly coarsened during the high-temperature compression. It is further suggested that the evolutionary behavior of the grain structure of copper is similar under ultrasonic and thermal fields.

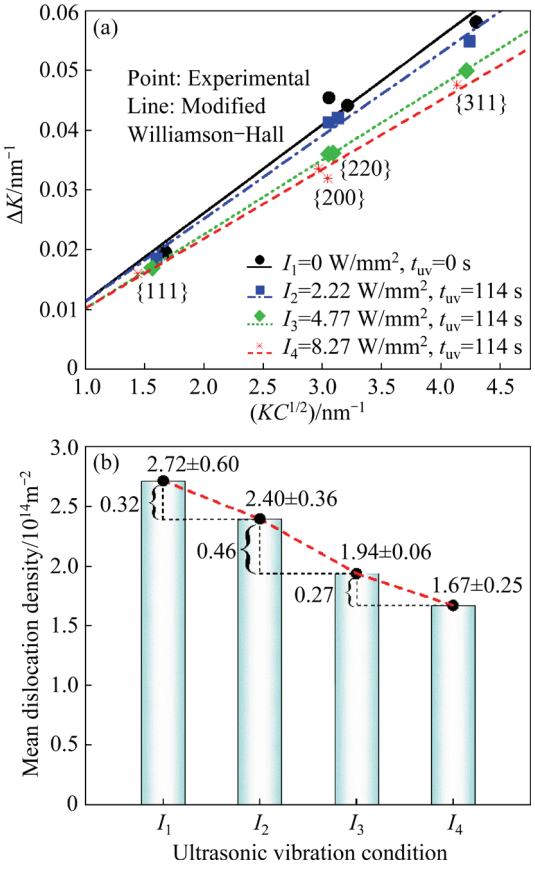

Fig. 3 Modified Williamson–Hall plot (a) and mean dislocation density (b)

In combination with the above experimental phenomena, the results indicate that the residual softening effect is caused by the combination of the additional evolution of grain size and dislocation density induced by the UV, which provides some support for coupling the evolution of dislocation density and grain size to describe the residual softening effect of the UV.

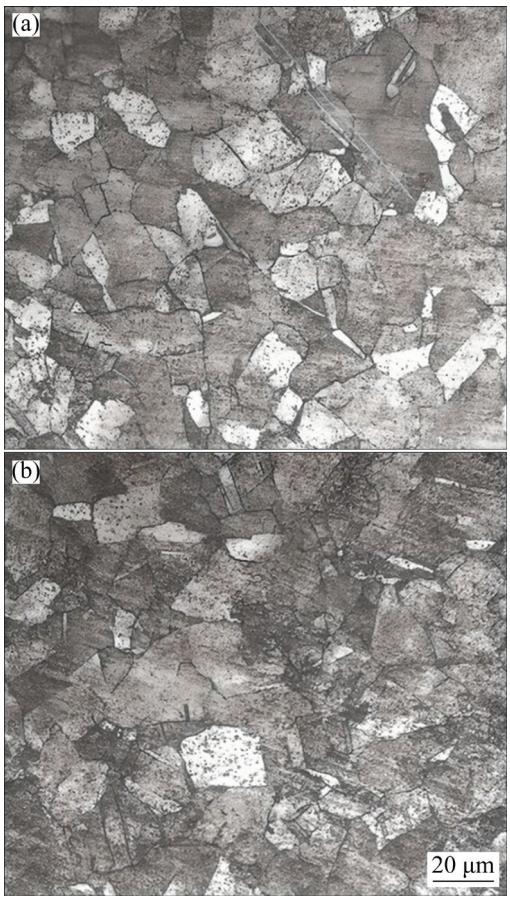

Fig. 4 Optical images of samples: (a) Deformed without UV; (b) Deformed with ultrasonic energy intensity of 4.77 W/mm^2 and duration of 114 s

4 Parameter determination and application of model

4.1 Parameter determination

In this section, the material parameters of the UV constitutive model for OFHC copper are determined. The parameters used in the unified constitutive model can be divided into three categories.

First, some of the parameters in the model, which are not related to the vibrations, are obtained from the literature and are given in Table 2. Since it is difficult to independently estimate the dislocation density in the grain boundary or grain involved in the dislocation emission energy, the approximate assumption is adopted in this study that the saturated dislocation density is regarded as the value of the dislocation density in the grain boundary while the dislocation density in the grain is determined by the initial dislocation density of the fully annealed microstructure [7].

Second, the parameters involved in the vibrations can be obtained from the results of the curve-fitting between the model and experiment. WANG et al [22] pointed out that the contribution of stress superimposition to stress reduction is approximately 0.2 compared with the acoustic softening. Additionally, the non-thermally activated contribution to flow stress can be estimated by the x-intercept on the Haasen plot. The results of KASCHNER and GIBELING [36] indicated that the contribution of the non-thermally activated stresses to flow stresses is approximately 0.5 through low cycle fatigue test with copper. Then, by combining the values in Table 2 with the experimental data, the dependence of the stress reduction due to the softening effect on the ultrasound intensity can be calculated using the equations in our model. The results are shown in

Table 2 Parameters not involving ultrasonic energy field for OFHC copper

Parameter	Value	Reference
ΔG_0/J	2.82×10^{-19}	[32]
K/(J·K^{-1})	1.38×10^{-23}	[15]
μ/GPa	49.80	[33]
b/m	2.56×10^{-10}	[34]
ρ_{mc1}/(kg·m^{-3})	8960	[33]
$\dot{\varepsilon}_p$ /s^{-1}	1.76×10^{8}	[15]
τ_0/MPa	16.99	[15]
ξ_2	0.45	[20]
ρ_{gb}/m^{-2}	6.10×10^{15}	[35]
ρ_{gi}/m^{-2}	5.00×10^{12}	[35]

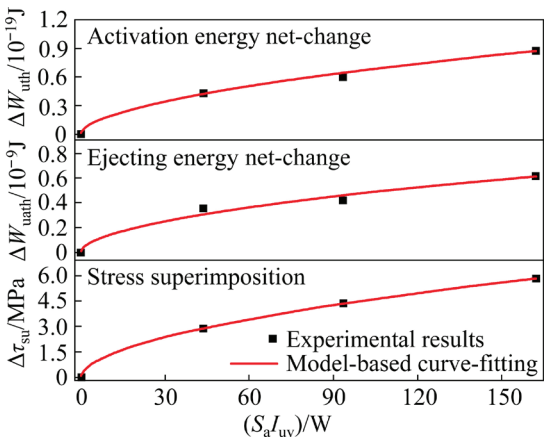

Fig. 5 Dependence of stress reduction due to softening effect on acoustic intensity

Fig. 5. The net energy change due to the UV is relatively consistent with the exponential function. As given in Table 3, the parameters associated with the softening effect are obtained from the model-based curve fitting.

In this study, the UV impact factor is defined as $\eta_\rho=\rho_u/\rho_w$ ($\eta_d=d_u/d_w$, where the subscripts "u" and "w" represent UV and without UV, respectively) in the same deformation. The impact factors are output for different acoustic intensities and vibrational duration, as shown in Fig. 6. The additional evolution behavior of the UV-induced mean the dislocation density and grain size is in relatively good agreement with the logistic function curve. Therefore, the parameters related to the acoustic residual effect are obtained by fitting the nonlinear curves and comparing them with Eqs. (18) and (23). Table 3 gives the values of the parameters.

Finally, since the unified constitutive model represented in Eq. (25) is a group of highly coupled nonlinear differential equations, the remaining material constants can be resolved through an optimization strategy. The genetic algorithm-based objective optimization (GAO) can obtain the overall optimum parameters and has been widely employed in various engineering optimization domains [37]. In this study, this optimization process is implemented by developing a MATLAB program, and the optimal parameters are obtained by comparison with experimental data. The optimization details can be found in the techniques specified by LIN and YANG [38]. The optimization results are given in Table 4.

Table 3 Parameters involving ultrasonic energy field for OFHC copper

Parameter	Value	Parameter	Value
β_{uth}	5.2012×10^{-21}	η_ρ^0	0.0154
n_{uth}	0.5540	η_ρ^S	0.4246
β_{uath}	4.0466×10^{-11}	r_ρ	1.0064×10^{-8}
n_{uath}	0.5350	η_d^0	1.0359
ξ_{su}	0.3833	η_d^S	2.0282
n_{su}	0.5351	r_d	4.1331×10^{-10}

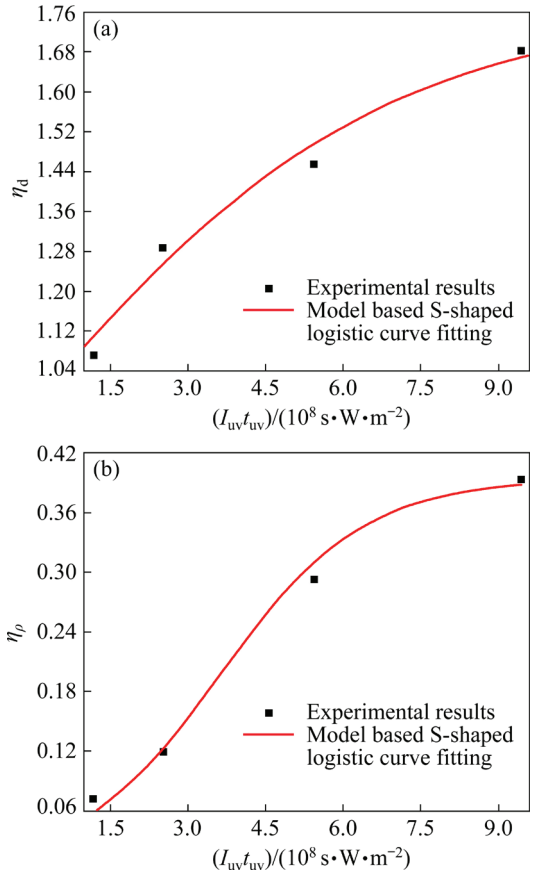

Fig. 6 Dependence of impact factors on acoustic intensity and duration: (a) η_d; (b) η_ρ

Table 4 Final optimized results of material constants for OFHC copper

Parameter	Value	Parameter	Value
p	0.8854	$\varsigma_{\bar{\rho}0}$	0.0437
q	1.1021	α_2	1.5543
β_2	4.6714×10^{-4}	α_1	10.5037
ς_{d2}	0.0113	$\varsigma_{\bar{\rho}1}$	1.6204
β_3	0.0655	$\xi_{\dot{S}}$	3.5508×10^{-2}
ς_{d3}	0.1855	β_4	0.6737
ς_{d4}	0.7839	$\bar{\rho}_c$	0.2644
ς_{d5}	0.7729	$n_{\dot{S}}$	0.6556
α_0	0.6153	ξ_1	0.7672
β_x	8.7586×10^{-4}		

4.2 Application of model

The plastic flow behaviors under different deformation conditions are predicted using the optimal parameters. The flow stress predicted by the model is compared with the experimental data, as shown in Fig. 7. It is shown that the model effectively captures the softening and residual softening behavior of OFHC copper at different sound intensities. However, it is worth noting that there are nearly linear ramp segments in the flow stress after the UV stops, which is the elastic recovery process after the deformed system has lost

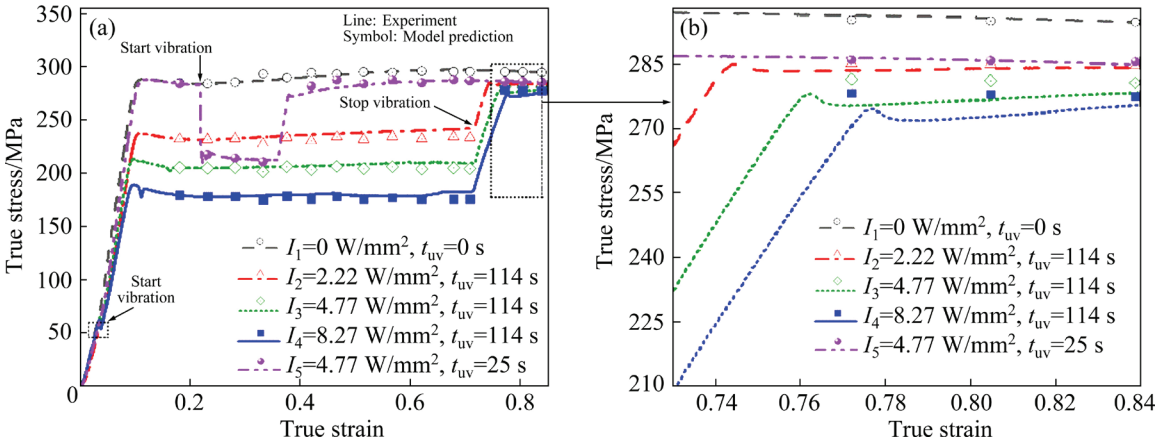

Fig. 7 True stress–strain curves for OFCH copper from experiments and modelling

the ultrasound energy. This model only considers the plastic flow phase of the material and therefore cannot predict the elastic recovery process.

In order to reflect the prediction capability of the model more intuitively, the statistical parameters [39] including the root mean squared error (RMSE) and correlation coefficient (R), are used to quantitatively analyze the flow stresses. These parameters are given in Eqs. (27) and (28), respectively:

$$\mathrm{RMSE}=\sqrt{\sum_{i=1}^{N}\left(E_i-C_i\right)^2/N} \tag{27}$$

$$R=\sum_{i=1}^{N}\left(E_i-\bar{E}\right)\left(C_i-\bar{C}\right)/\left[\sqrt{\sum_{i=1}^{N}\left(E_i-\bar{E}\right)^2}\sqrt{\sum_{i=1}^{N}\left(C_i-\bar{C}\right)^2}\right] \tag{28}$$

where N represent the number of data, E_i and C_i are the experimental and calculated data, respectively, $\bar{E}$ and $\bar{C}$ represent the averages of the experimental and calculated data, respectively. The RMSE and R of predicted results (I_4=8.27 W/mm², and t_{uv}=114 s; I_5=4.77 W/mm², and t_{uv}=25 s) are 2.55 MPa and 3.79 MPa, and 0.9988 and 0.9905 respectively. The calculated results show that the predicted flow stresses are in good agreement with the experimental ones. The deviation may be due to the model ignoring the influence of inhomogeneous dislocation distribution and grain shape on the flow stresses. In addition, the residual softening behavior of OFHC copper is overestimated by the model (Fig. 7(b)). This condition may be caused by the assumption that all dislocations are mobile dislocations, which is inconsistent with the actual deformation. As pointed out by FAN et al [40], the relationship between strain rate and the collective dynamics within dislocations still has many fundamental problems that have not been properly answered and still need to be systematically investigated. In addition, in the future work, the model will also be applied to aluminum alloy and stainless-steel materials to assess the feasibility of the developed constitutive model to FCC metals.

5 Discussion

The UV softening behavior is caused by the periodic loading/unloading of the specimens caused by mechanical vibration at ultrasonic frequency, which results in a decrease in the average load. However, the stress superposition mechanisms do not alter the plastic deformation, which makes it impossible to explain the additional evolution of the dislocation density and the grain size of copper induced by the UV in the same strain conditions. It was also proven by DAUD et al [41] considering elastic relaxation.

Microscopically, the plastic deformation can be understood as the movement and interaction of dislocations under the rate control mechanisms [15]. As the amplitude of the UV is on the order of microns, this periodic loading/unloading is an elastic deformation of the material. Compared to conventional metal forming, the UV can achieve the same deformation with less load. The total energy required for the specimen to reach the same

deformation is not changed according to the law of conservation of energy, and it is only transformed into another form. Based on the energy minimum principle, the superposition of the UV changes the bonding forces among atoms and allows atoms to be in a low-energy state. Therefore, regarding the crystal plasticity model of Eqs. (5) and (9), another reason of the softening behavior is that the superposition of the UV reduces the potential barriers that hinder the dislocation movement, which makes it easier for dislocations to move. The superimposition of UV increases the capacity for dislocation motion, which then induces different degrees of additional evolution of the internal structure as the sample is exposed to the acoustic field for extended periods of time. So, after the superimposition of UV ceases, the acoustic residual phenomenon of the material occurs.

However, as the model shows, the acoustic residual phenomenon cannot be described simply by modelling the evolution of a single factor (dislocation density). From the experimental results of this study and previous studies, it is found that FCC metals with different stacking fault energies exhibit different results in microstructural evolution during UV assisted forming, which results in different residual phenomena. Therefore, the different acoustic residual phenomena are related to the patterns of dislocation motion, recrystallization, and grain growth with different stacking fault energies. For copper with medium stacking fault energy, the movement of the dislocation splitting into two partial dislocations during deformation is favorable. Recrystallization behavior occurs when the dislocation density of the sample increases to a certain critical value during UV assisted forming and the local density difference is high enough. The grains are relatively fine and the internal dislocation density is also relatively small when the recrystallization is just completed. Besides, the other reason for the decrease in dislocation density can be the ultrasound-induced increase in dislocation mobility, leading to an increase in the probability of opposite dislocation encounters and annihilation [42].

With the extension of UV application time, some grains exhibit sudden growth behavior, while other grains remain small and finally are swallowed by the large grains, resulting in a relatively large mean grain size in the sample. The grain boundary mobility depends on the orientation relationship between the growing grain and the surrounding matrix [43] and the migration speed of grain boundaries increases with the increase of orientation difference. Hence, the UV can change the misorientation in the local area near the grain boundary, increasing the rate of grain boundary migration, and inducing preferential grain growth, which results in the rapid growth of some grains. DESHPANDE et al [26] used EBSD and transmission electron microscope (TEM) to investigate the microstructure evolution of copper during UV assisted compression and found that the UV increased the local misorientation near the grain boundaries and induced the recrystallisation behavior of copper. KANG et al [10] indicated by using EBSD analysis of the plastic behavior of copper in ultrasound-assisted tensile tests that UV promoted the meritocratic orientation of the grains. The above research results and the decreasing trend of the average dislocation density (shown in Fig. 3) estimated by using XRD in this study could provide evidence for it to a great extent. Therefore, after the cessation of UV, a residual softening behavior of copper occurred on the macroscopic stress−strain curve.

However, the exact physics between the UV and these effects is still unclear and needs further investigation in the future work. In this study, the effect of UV on microstructure is included in the phenomenological formulation (Eqs. (22) and (24)). The density and type of dislocations, the size and shape of grains, and the spatial distribution are not considered cooperatively, resulting in the existence of some empirical parameters in the model, which is also the direction of optimization and development of the model in the future. In general, the model provides new modelling mechanisms for describing the plastic flow behavior of FCC metal in the UV.

6 Conclusions

(1) The correlation among the ultrasonic energy field, dislocation density evolution and grain evolution are established by considering dislocation

movement and accumulation, grain growth and dynamic recrystallisation under UV.

(2) The acoustic softening effect is caused by ultrasound energy fields altering the atomic bonding forces, which results in a reduction in the potential barrier to dislocation movement.

(3) Stacking fault energy, dislocation density and grain size are critical factors in determining different acoustic residual effects.

(4) The predictions of the model for the flow stress are in good agreement with the experimental data, with a maximum root mean square error of 3.79 MPa, which provides a satisfactory description of the softening behavior and residual behavior of OFHC copper under UV.

CRediT authorship contribution statement

Peng-fei SONG: Conceptualization, Methodology, Validation, Formal analysis, Investigation, Software, Writing − Original draft; **Miao-yan CAO:** Investigation, Formal analysis, Writing − Review & editing, Funding acquisition, Supervision; **Han HU:** Formal analysis, Software, Writing − Review & editing; **Ji-ye CHEN:** Formal analysis, Writing − Review & editing, Supervision; **Min FU:** Formal analysis, Writing − Review & editing.

Declaration of competing interest

The authors declare that they have no known competing financial interests or personal relationships that could have appeared to influence the work reported in this paper.

Acknowledgments

The research work was supported by the National Natural Science Foundation of China (Nos. 51775480, 51605420); the Natural Science Foundation of Hebei Province, China (No. E2018203143).

References

[1] SHAO Guang-da, LI Hong-wei, ZHAN Mei. A review on ultrasonic-assisted forming: Mechanism, model, and process [J]. Chinese Journal of Mechanical Engineering, 2021, 34(1): 33−99.

[2] YAO Zhe-he, KIM G Y, WANG Zhi-hua, LEANN F, ZOU Qing-ze, MEI De-qing, CHEN Zi-chen. Acoustic softening and residual hardening in aluminum: Modeling and experiments [J]. International Journal of Plasticity, 2012, 39: 75−87.

[3] CONRAD H. The athermal component of the flow stress in crystalline solids [J]. Materials Science and Engineering, 1970, 6: 265−273.

[4] SEDAGHAT H, XU Wei-xing, ZHANG Liang-chi. Ultrasonic vibration-assisted metal forming: Constitutive modelling of acoustoplasticity and applications [J]. Journal of Materials Processing Technology, 2019, 265: 122−129.

[5] ZHAO Wen-zhen, WU Chuan-song. Constitutive equation including acoustic stress work and plastic strain for modeling ultrasonic vibration assisted friction stir welding process [J]. International Journal of Machine Tools and Manufacture, 2019, 145: 103434.

[6] MENG B, CAO B N, WAN M, WANG C J, SHAN D B. Constitutive behavior and microstructural evolution in ultrasonic vibration assisted deformation of ultrathin superalloy sheet [J]. International Journal of Mechanical Sciences, 2019, 157/158: 609−618.

[7] WANG Xin-wei, WANG Chun-ju, LIU Yang, LIU Chen, WANG Zhen-long, GUO Bin, SHAN De-bin. An energy based modeling for the acoustic softening effect on the Hall−Petch behavior of pure titanium in ultrasonic vibration assisted micro-tension [J]. International Journal of Plasticity, 2021, 136: 102879.

[8] HAGHAYEGHI R. Effect of external forces on microstructural evolution and mechanical properties of high pressure die cast AA5754 alloy [J]. Transactions of Nonferrous Metals Society of China, 2017, 27(2): 282−288.

[9] PADHY G K, WU C S, GAO S. Precursor ultrasonic effect on grain structure development of AA6061-T6 friction stir weld [J]. Materials & Design, 2017, 116: 207−218.

[10] KANG Jia-rui, LIU Xun, XU Ming-jie. Plastic deformation of pure copper in ultrasonic assisted micro-tensile test [J]. Materials Science and Engineering A, 2020, 785: 139364.

[11] LENNON A M, RAMESH K T. The influence of crystal structure on the dynamic behavior of materials at high temperatures [J]. International Journal of Plasticity, 2004, 20(2): 269−290.

[12] XIE Ke-wei, NIE Jin-feng, HU Kai-qi, MA Xia, LIU Xiang-fa. Improvement of high-temperature strength of 6061 Al matrix composite reinforced by dual-phased nano-AlN and submicron-Al_2O_3 particles [J]. Transactions of Nonferrous Metals Society of China, 2022, 32(10): 3197−3211.

[13] KIRCHNER H O K, KROMP W K, PRINZ F B, TRIMMEL P. Plastic deformation under simultaneous cyclic and unidirectional loading at low and ultrasonic frequencies [J]. Materials Science and Engineering, 1985, 68: 197−206.

[14] YANG Zhi-chao, ZHU Li-da, ZHANG Gui-xiang, NI Chen-bing, LIN Bin. Review of ultrasonic vibration-assisted machining in advanced materials [J]. International Journal of Machine Tools and Manufacture, 2020, 156: 103594.

[15] GAO C Y, ZHANG L C. Constitutive modelling of plasticity of fcc metals under extremely high strain rates [J]. International Journal of Plasticity, 2012, 32/33: 121−133.

[16] MEYERS M A. Dynamic behavior of materials [M]. New York: Wiley-Interscience, 1994: 230−239.

[17] KLEPACZKO J. Thermally activated flow and strain rate

history effects for some polycrystalline FCC metals [J]. Materials Science and Engineering, 1975, 18: 121−135.

[18] KOCKS U F. Thermodynamics and kinetics of slip [J]. Progress in Materials Science, 1975, 19: 1−291.

[19] MESSERSCHMIDT U. Dislocation dynamics during plastic deformation [M]. Heidelberg: Springer-Verlag Berlin, 2010: 180−187.

[20] BATA V, PERELOMA E V. An alternative physical explanation of the Hall−Petch relation [J]. Acta Materialia, 2004, 52: 657−665.

[21] ENSMINGER D, BOND L. Ultrasonics: Fundamentals, technologies, and applications [M]. Third ed. New York: CRC Press, 2020: 30−36.

[22] WANG C J, LIU Y, GUO B, SHAN D B, ZHANG B. Acoustic softening and stress superposition in ultrasonic vibration assisted uniaxial tension of copper foil: Experiments and modeling [J]. Materials & Design, 2016, 112: 246−253.

[23] JIANG Mao-yuan, DEVINCRE B, MONNET G. Effects of the grain size and shape on the flow stress: A dislocation dynamics study [J]. International Journal of Plasticity, 2019, 113: 111−124.

[24] LIN J, LIU Y, FARRUGIA D C J, ZHOU M. Development of dislocation-based unified material model for simulating microstructure evolution in multipass hot rolling [J]. Philosophical Magazine, 2005, 85(18): 1967−1987.

[25] MOOSBRUGGER J C. Continuum slip viscoplasticity with the Haasen constitutive model: Application to CdTe single crystal inelasticity [J]. International Journal of Plasticity, 1995, 11: 799−826.

[26] DESHPANDE A, TOFANGCHI A, HSU K. Microstructure evolution of Al6061 and copper during ultrasonic energy assisted compression [J]. Materials Characterization, 2019, 153: 240−250.

[27] LIN Jian-guo. Fundamentals of materials modelling for metals processing technologies: Theories and applications [M]. Europe: World Scientific Publishing Co Pte Ltd., 2015: 129−138.

[28] LI He, ZHAN Li-hua, HUANG Ming-hui, ZHAO Xing, ZHOU Chang, HU Li-bin, HU Zheng-gen, LIU De-bo. A unified constitutive model for multiphase precipitation and multi-stage creep ageing behavior of Al−Li−S4 alloy [J]. Transactions of Nonferrous Metals Society of China, 2021, 31(5): 1217−1234.

[29] UNGÁR T, GUBICZA J, RIBÁRIK G, BORBÉLY A. Crystallite size distribution and dislocation structure determined by diffraction profile analysis: Principles and practical application to cubic and hexagonal crystals [J]. Journal of Applied Crystallography, 2001, 34(3): 298−310.

[30] STOKES A R. A numerical Fourier-analysis method for the correction of widths and shapes of lines on X-ray powder photographs [J]. Proceedings (Physical Society (Great Britain): 1926), 1948, 61(4): 382−391.

[31] ZHANG Hong-ming, WANG Jing, CHEN Qiang, SHU Da-yu, WANG Chang-peng, CHEN Gang, ZHAO Zu-de. Study of dynamic recrystallization behavior of T2 copper in hot working conditions by experiments and cellular automaton method [J]. Journal of Alloys and Compounds, 2019, 784: 1071−1083.

[32] SIA N N, LUQUN N, TOMOO O. A constitutive model for fcc crystals with application to polycrystalline OFHC copper [J]. Mechanics of Materials, 1998, 30(4): 325−341.

[33] RUSINEK A, RODRÍGUEZ-MARTÍNEZ J A, ARIAS A. A thermo-viscoplastic constitutive model for FCC metals with application to OFHC copper [J]. International Journal of Mechanical Sciences, 2010, 52(2): 120−135.

[34] DING R, GOU Z X. Coupled quantitative simulation of microstructural evolution and plastic flow during dynamic recrystallization [J]. Acta Materialia, 2001, 49: 3163−3175.

[35] VOYIADJIS G Z, ABED F H. Effect of dislocation density evolution on the thermomechanical response of metals with different crystal structures at low and high strain rates and temperatures [J]. Archives of Mechanics, 2005, 57: 299−343.

[36] KASCHNER G C, GIBELING J C. Evolution of dislocation glide kinetics during cyclic deformation of copper [J]. Acta Materialia, 2002, 50: 653−662.

[37] WU Yong, FAN Rong-lei, QIN Zhong-huan, CHEN Ming-he. Shape controlling and property optimization of TA32 titanium alloy thin-walled part prepared by hot forming [J]. Transactions of Nonferrous Metals Society of China, 2021, 31(8): 2336−2357.

[38] LIN J, YANG J B. GA-based multiple objective optimisation for determining viscoplastic constitutive equations for superplastic alloys [J]. International Journal of Plasticity, 1999, 15: 1181−1196.

[39] LI Xin, SHAN Guang-cun, ZHAO Hong-bin, SHEK Chan-Hung. Domain knowledge aided machine learning method for properties prediction of soft magnetic metallic glasses [J]. Transactions of Nonferrous Metals Society of China, 2023, 33(1): 209−219.

[40] FAN H D, WANG Q Y, EI-AWADY J A, RAABE D, ZAISER M. Strain rate dependency of dislocation plasticity [J]. Nature Communications, 2020, 12: 1845.

[41] DAUD Y, LUCAS M, HUANG Z H. Modelling the effects of superimposed ultrasonic vibrations on tension and compression tests of aluminium [J]. Journal of Materials Processing Technology, 2007, 186(1/2/3): 179−190.

[42] DUTTA R K, PETROV R H, DELHEZ R, HERMANS M J M, RICHARDSON I M, BÖTTGER A J. The effect of tensile deformation by in situ ultrasonic treatment on the microstructure of low-carbon steel [J]. Acta Materialia, 2013, 61: 1592−1602.

[43] JENSEN D J. Growth rates and misorientation relationships between growing nuclei/grains and the surrounding deformed matrix during recrystallization [J]. Acta Metallurgica et Materialia, 1994, 43: 4117−4129.

超声振动下 FCC 金属统一本构模型及其在无氧高导热铜的应用

宋鹏飞[1,2]，曹秒艳[1,2]，胡 晗[1,2]，陈吉业[3]，付 敏[1,2]

1. 燕山大学 机械工程学院，秦皇岛 066004；
2. 燕山大学 河北省轻质结构装备设计与制备工艺技术创新中心，秦皇岛 066004；
3. School of Civil Engineering and Surveying, University of Portsmouth, Portsmouth PO1 3AH, UK

摘 要：建立统一本构模型，预测面心立方金属(FCC)超声振动(UV)辅助成形塑性流动行为。该模型基于超声能场下的位错动力学并结合应力叠加机制描述 UV 软化行为。考虑位错密度、晶粒尺寸和超声能场的相互作用，以位错密度和晶粒尺寸作为内部状态变量建立模型，预测 UV 辅助成形的残余行为。开展无氧高导热(OFHC)铜 UV 辅助压缩试验来验证该模型的预测能力。结果表明，OFHC 铜在 UV 下表现出明显的软化行为和残留软化行为，模型预测与实验结果吻合较好，有效反映铜的软化效应和残余效应。

关键词：本构建模；超声振动；声软化行为；压缩；铜

(Edited by Bing YANG)